Simultaneous Precipitation of Sub-Relativistic Electron Microburst and Pulsating Aurora Electrons

T. Namekawa[1,2], T. Mitani[1], K. Asamura[1], Y. Miyoshi[3], K. Hosokawa[4], M. Lessard[5], C. Moser[5], A. J. Halford[6], T. Sakanoi[7], M. Kawamura[7], M. Nose[3], R. Nomura[1], M. Teramoto[8], M. Shumko[9], K. Lynch[10], A. N. Jaynes[11], M. G. McHarg[12]

[1]Japan Aerospace Exploration Agency, Japan, [2]The University of Tokyo, Japan, [3]Nagoya University, Japan, [4]The University of Electro-Communications, Japan, [5]University of New Hampshire, USA, [6]NASA Goddard Space Flight Center, USA, [7]Tohoku University, Japan, [8]Kyushu Institute of Technology, Japan, [9]University of Maryland, USA, [10]Dartmouth College, USA, [11]University of Iowa, USA, [12]United States Air Force Academy, USA

Corresponding author: Taku Namekawa (namekawa@stp.isas.jaxa.jp)

Key Points:

- A sounding rocket observed simultaneously precipitating sub-relativistic electron microbursts and pulsating auroral electrons.
- 250–580 keV electron precipitations were detected 0–30 ms after 180–320 keV electron precipitations in a single auroral patch.
- The energy dispersion of observed electrons is consistent with the theory that they are due to chorus waves propagating to higher latitudes.

Abstract

We have identified for the first time an energy-time dispersion of precipitating electron flux in a pulsating aurora patch, ranging from 6.7 keV to 580 keV, through simultaneous in-situ observations of sub-relativistic electrons of microburst precipitations and lower-energy electrons using the LAMP sounding rocket launched from the Poker Flat Research Range in Alaska. Our observations reveal that precipitating electrons with energies of 180-320 keV were observed first, followed by 250-580 keV electrons 0-30 ms later, and finally, after 500-1000 ms, 6.7-14.6 keV electrons were observed. The identified energy-time dispersion is consistent with the theoretical estimation that the relativistic electron microbursts are a high-energy tail of pulsating aurora electrons, which are caused by chorus waves propagating along the field line.

Plain Language Summary

A sounding rocket observes both sub-relativistic electron precipitations called microbursts and electrons causing pulsating auroras simultaneously. The detection time differences of these electrons in an energy range from 6.7 keV to 580 keV are identified at the rocket altitude. A possible mechanism for generating these precipitations is the resonance scattering of electrons by chorus waves propagating from the equatorial plane to higher latitudes along the field line. The observed energy energy-time dispersion of precipitating electrons is consistent quantitatively with the theory about wide energy electron precipitations caused by chorus waves propagating toward higher latitudes.

1 Introduction

Microburst precipitations of relativistic/sub-relativistic electrons are observed as a train of bursty precipitations of high-energy (several hundred keV to several MeV) electrons into the Earth's atmosphere with typical time scales less than a second [e.g., Nakamura et al., 1995; Blake et al., 1996; Datta et al., 1997; Kurita et al., 2016; Douma et al., 2017; Lorentzen et al., 2001; O'Brien et al., 2003; Shumko et al., 2018, 2021a, 2021b; Kawamura et al., 2021]. The spatial scale of a microburst is typically tens of kilometers, and the time scale of a single burst is about 100 ms [Shumko et al., 2018, 2021b]. Microbursts are often observed on the dawn-side (MLT=0–12 h) at L=3–8, and their occurrence frequency increases as geomagnetic activity increases [e.g., Blum et al. 2015, Lorenzen et al. 2001, O'Brien et al. 2003, Douma et al. 2017].

It is suggested that microbursts are vital loss mechanisms of the outer radiation belt electrons [e.g., Thorne et al., 2005; Clilverd et al., 2006; Dietrich et al., 2010; Lorentzen et al., 2001]. In addition, the relativistic electron microbursts possibly make a significant impact on the Earth's upper atmosphere. Relativistic electron precipitations are estimated to cause 20–30% increase of atmospheric nitrogen oxide (NOx) and 10–20% depletion of upper mesospheric ozone (O_3) [Miyoshi et al., 2015a, 2021; Seppälä et al., 2018; Duderstadt et al., 2021; Verronen et al., 2021]. Because of these close relationships between the radiation belt and the upper/middle atmosphere, we need to understand characteristics, generation conditions as well as mechanisms of microbursts.

The microbursts are suggested to be caused by pitch angle scattering due to magnetospheric whistler-mode chorus waves propagating from the magnetic equator to higher magnetic latitudes [e.g., Miyoshi et al., 2020]. Theoretically, the chorus waves can scatter relativistic/sub-relativistic electrons when they propagate to high latitudes along the field line because the resonance energy of chorus waves becomes higher [Horne & Thorne, 2003; Miyoshi

et al. 2010, 2015a, 2020]. Microbursts and chorus waves have similar time scales and spatial distributions in L-value and MLT [e.g., Lorenzen et al., 2001, Nakamura et al., 2000]. Chorus waves and microbursts were also simultaneously observed on nearby magnetic field lines or same satellite [Breneman et al. 2017; Oliver and Gurnett, 1968].

Pulsating aurora is a type of diffuse aurora that exhibits intermittent modulation of luminosity whose period is typically several seconds. The precipitation of several to ~100 keV electrons scattered by the chorus waves causes the pulsating auroral emission in the Earth's auroral ionosphere [e.g., Miyoshi et al., 2010, 2015b, 2021; Kasahara et al., 2018; Ozaki et al., 2019; Hosokawa et al., 2020]. A few Hz internal modulations are sometimes embedded in the main pulsation of the pulsating aurora. This time scale is very similar to that of rising tone elements of chorus waves and a single burst of a microburst. For higher-energy electrons, Sandahl et al. (1980) observed precipitations of about 140 keV electrons into the ionosphere during pulsating aurora by a sounding rocket experiment. Radar observations also indicated that relativistic/sub-relativistic electrons precipitate into the middle atmosphere in association with pulsating auroras [e.g., Miyoshi et al., 2015b, 2021; Oyama et al., 2017]. However, direct observational evidence on the relationship between microbursts and pulsating auroral electrons has not yet been obtained.

Recently, based on the theory [Miyoshi et al., 2010; Saito et al., 2012], Miyoshi et al. (2020) proposed a model in which chorus waves propagating along the field line cause electron scattering in a wide energy range, and both pulsating aurora electrons and relativistic/sub-relativistic electron microbursts are the same origin caused by the propagation of chorus waves. Kawamura et al. (2021) and Shumko et al. (2021a) reported that relativistic electron microbursts occurred with the pulsating auroral emission, which is consistent with the model proposed by Miyoshi et al. (2020). Another clue to confirm this model is the characteristic energy-time dispersion of the precipitating electron fluxes. The model predicts 'inverse' energy-time dispersion of the precipitating electron fluxes; electrons with energies a few hundred keV arrive at the ionosphere before higher-energy (MeV) electrons. This feature is caused by the propagation delay of chorus waves from the magnetic equator to higher latitudes, increasing the resonance energy of electrons due to increased background magnetic field strength along the wave propagation path, and elongation of the travel distance of electrons from the scattering point to the ionosphere. Kawamura et al. (2021) reported this inverse energy-time dispersion of precipitating electron fluxes in a patch structure of pulsating aurora by using simultaneous observations of high-energy electrons and auroral emissions with the FIREBIRD-II satellite and ground-based auroral imagers. However, they showed no direct observations of lower-energy electrons causing the pulsating aurora.

This paper reports the first in-situ observation of the energy-time dispersion of precipitating electrons of microbursts and pulsating auroras obtained by the LAMP sounding rocket experiment. We analyzed the precipitating electron data covering from 6.7 keV up to MeV range. We successfully detected the timing differences of the electron precipitations for different energies in a pulsating auroral patch. We also performed a model calculation about the energy-time dispersion of electron fluxes, taking into account the interactions between chorus waves and electrons, and compared it with the LAMP observations. We describe the instrumental setup in the next section, followed by observational results in Section 3. Discussion and summary are provided in Sections 4 and 5, respectively.

2 Instrumentation

The Loss through Auroral Microburst Pulsation (LAMP) mission is a US-Japan sounding rocket experiment designed to observe the microburst electrons and the pulsating auroras simultaneously. We used the data obtained by a high-energy electron detector (HEP: High Energy Particle detector), a low-energy electron detector (EPLAS: Electron PLASma detector), auroral imagers (AIC: Auroral Imaging Camera), and a magnetometer (MIM: Magneto-Impedance Magnetometer). LAMP was launched from Poker Flat Research Range, Alaska (65.1°N, 147.5°W in geographic coordinates; 65.8°N 95.2°W in geomagnetic coordinates; L = 5.94) at 11:27:30 UT on March 5, 2022. MLT of Poker Flat at the launch was 0.1 hr.

HEP is an improved version of the detector installed in a previous sounding rocket experiment [Namekawa et al., 2021]. HEP consists of a mechanical collimator, eight-layered silicon semiconductor detectors (SSDs), which measure the energies of incident particles, and an anti-coincidence sensor used to remove the effects of cosmic rays. HEP can measure 975 keV electrons from ^{207}Bi radiation source with an energy resolution $\Delta E = 53.5$ keV. The anti-coincidence sensor consists of a plastic scintillator and four avalanche photodiodes (APDs). A part of cosmic rays penetrating through the SSDs emit photons inside the plastic scintillator surrounding the SSDs, and the APDs detect these photons. Then, the contribution of cosmic rays can be eliminated by the detection signals generated by the APDs. HEP was mounted on the top of the rocket so that the center of the field of view of HEP was parallel to the thrust axis of the rocket, which was controlled to be parallel to the local geomagnetic field.

EPLAS is an electron energy spectrum analyzer that covers 5 eV to 15 keV with 42 energy steps. EPLAS has a 360-degree planar field of view divided by 36 angular bins. The sampling time of EPLAS for one energy step is 1 ms, providing a 2-D velocity distribution function every 42 ms. AIC consists of two high-speed CMOS monochromatic imagers. We used images obtained by Sensor 1 of AIC (AIC S1) that was sensitive to photons of N_2 1PG emission of auroras with a 20 nm bandpass filter centering at 670 nm with a frame rate of 9.5 Hz. N_2 1PG emission is the typical permitted line of auroral emission in the ionospheric E-region. The field of view and angular resolution of AIC S1 are 27° × 27° and 0.5° × 0.5°, respectively. MIM is a triaxial magnetometer based on the magneto-impedance effect. We calculated the pitch angles of observed electrons using MIM data.

3 Observation

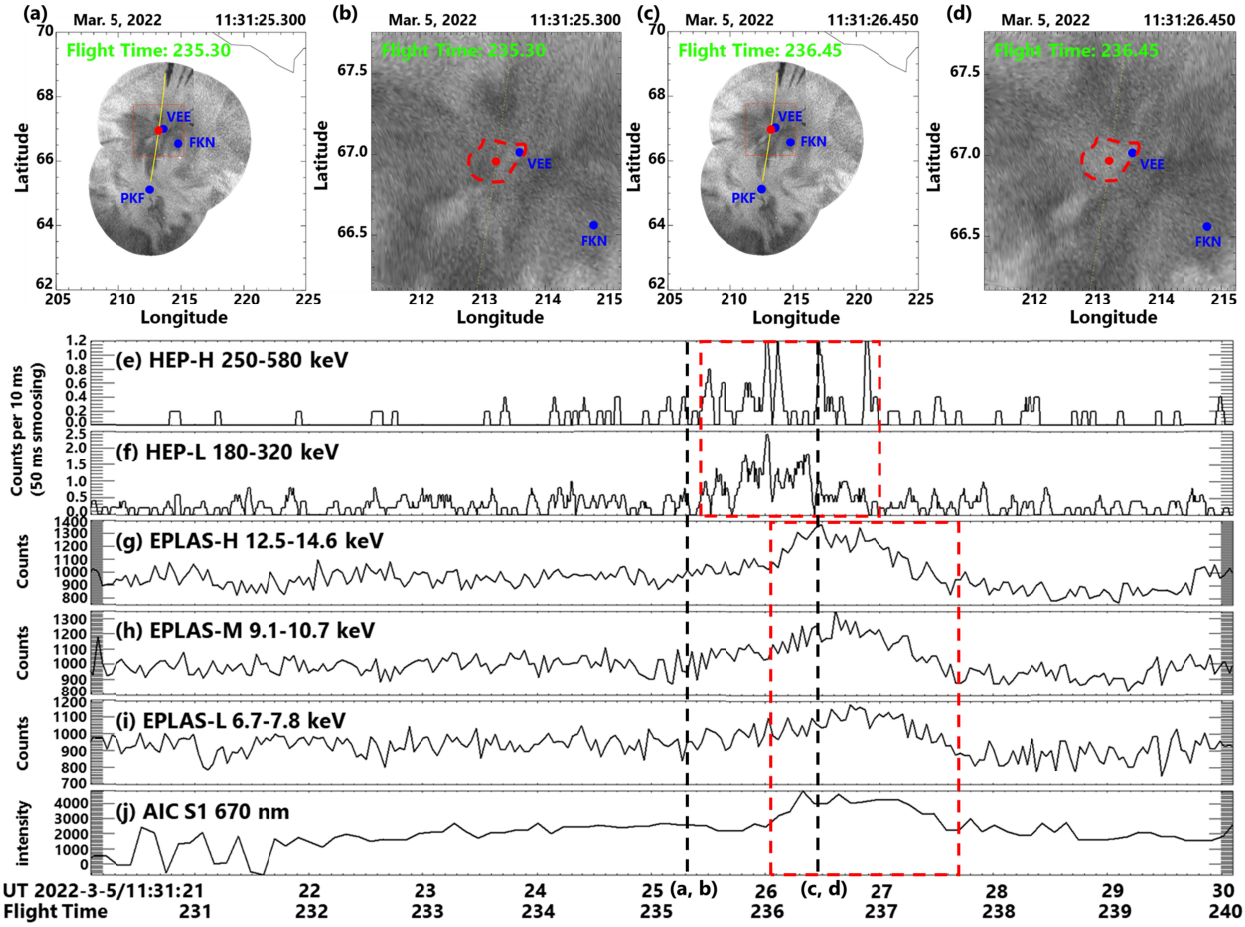

Figure 1. (a)-(d) Mosaic image of all-sky imagers captured at Poker Flat Research Range (PFRR), Fort Yukon (FKN), and Venetie (VEE). Red dots indicate the footprint of the LAMP sounding rocket at 100 km altitude. Yellow lines indicate the trajectory of the footprint of the LAMP sounding rocket. The mapped altitude was 100 km. (e) and (f): Count rate of precipitating electrons observed by HEP. Data are plotted in 10 ms intervals, where running averages over 50 ms are applied. (g)-(i): Count rate of electrons measured by EPLAS, where time resolution is 42 ms. (j) Emission intensity of photons (670 nm) at the magnetic footprint (altitude of 100 km) of the position of the rocket. Data are retrieved from images obtained by AIC S1. The black dotted lines on panels (e)-(j) correspond to the observation times of panels (a)-(d). The red dotted boxes on panels (e)-(j) correspond to the time range when a microburst train, a pulsating auroral patch and a low-energy electron precipitation train were observed.

A ground-based all-sky EMCCD imager operated at Venetie, which is located near below the magnetic footprint of the apex of the rocket trajectory, observed an auroral patch at 236 s from the launch of LAMP (Figures 1a-1d). The footprint of LAMP (red dot) was located within this patch, and the rocket was flying at an altitude of 388 km. The L-value was 7.0. Figures 1e-1f show the count rate of precipitating electrons observed by HEP plotted by 10ms intervals, with running averages over 50 ms. The center of the field of view of HEP pointed to 2.1 degrees off

the opposite direction of the local geomagnetic field. Since the field of view of HEP is 45.2° × 45.2°, the electrons with pitch angles between 0° and 32.6° could be detected. We apply labels HEP-H (HEP-High) and HEP-L (HEP-Low) for observed electron count rates of energy channels 250–580 keV and 180–320 keV, respectively. Figures 1g-1i show the count rate of precipitating electrons observed by EPLAS with a time resolution of 42 ms, where the count rate is summed over all the azimuthal channels of the instrument. Again, we apply labels EPLAS-H (EPLAS-High), EPLAS-M (EPLAS-Medium), and EPLAS-L (EPLAS-Low) for electron count rates of energy channels 12.5–14.6 keV, 9.1–10.7 keV, and 6.7–7.6 keV, respectively. Figure 1j shows the auroral emission intensity (wavelength at 670 nm) at the magnetic footprint of the rocket, observed by AIC S1 with a time resolution of 105 ms. Since AIC S1 looked downward from the rocket, reflected photons from the ground surface were also detected. The photon count rate due to the reflection has been estimated and subtracted in Figure 1j. The black dotted lines in Figures 1e-1j correspond to the observation times of the auroral images shown in Figures 1a-1b and Figures 1c-1d, respectively. The red dotted box in Figures 1e-1f corresponds to the time range when a microburst train was observed, and the red dotted box in Figures 1g-1j corresponds to the time range when a pulsating auroral patch and a low-energy electron precipitation train were observed.

Figures 1g-1j show that the EPLAS-H/M/L electron counts increase with the auroral intensity enhancement. These electrons contribute to the main pulsation of the pulsating aurora [Miyoshi et al., 2015b]. In Figures 1g-1i, modulations are embedded in the electron count enhancements of EPLAS-H/M/L. It is clear from Figures 1e-1i that the increases in HEP-H/L electron counts preceded those of EPLAS-H/M/L electrons. Figures 1g-1i also show that several spiky enhancements with a short duration, i.e., microbursts, are embedded in the microburst train. There appears to be a correspondence between the peaks in the microburst train of HEP-H/L and the modulations in the main pulsation of EPLAS-H/M/L. The electron counts observed by EPLAS show an energy-time dispersion that is similar to typical flux variations of pulsating auroral electrons reported in the previous studies [Miyoshi et al., 2010, 2015b; Nishiyama et al., 2011].

Here, we identify the difference in the arrival timing of the same microbursts observed by HEP-H and HEP-L in a more objective way. Figures 2a and 2c show the electron count rates (same as Figures 1e and 1f) together with smoothed values by applying 110 ms window sliding average. Figures 2b and 2d show the second time derivatives of the smoothed count rates, and the standard deviations of the second time derivatives for HEP-L and HEP-H, respectively. By using the second time derivative, the background can be subtracted without arbitrariness, and the locations of the peaks can be determined from the locations of their local minima. We applied the Savitzky-Golay method to calculate the smoothing, its second derivatives, and the standard deviations of the second derivatives. The standard deviations of the second time derivatives plotted in Figures 2b and 2d are sign-reversed for comparison with the local minima of the second time derivatives. The arrival timings of microbursts observed by the HEP-H and HEP-L were determined as the timings when the second time derivatives take local minima, and their absolute values are greater than the standard deviations. Only bursts with 0.6 counts per 10 ms or more were used in this analysis. The blue and red dotted lines show the timing of the microbursts at the HEP-L (Figures 2a and 2b) and the HEP-H (Figures 2c and 2d), respectively. We identified seven events in which the microburst at the HEP-H appears in close proximity to the microburst at the HEP-L. Red triangles in Figure 2c show the appearance timings of the identified seven microbursts of HEP-H. The HEP-L microbursts precede the HEP-H microbursts

by 13.3 ms on average over six events out of the seven events (as shown with red triangles). Note that the time lag between the microbursts is unclear in the remaining event. Assuming a normal distribution with an average of 13.3 ms and a variance of 306.7 ms^2 as the occurrence distribution of time differences between microbursts at HEP-L and HEP-H, it was found that 78% of microbursts at HEP-L appeared before those at HEP-H.

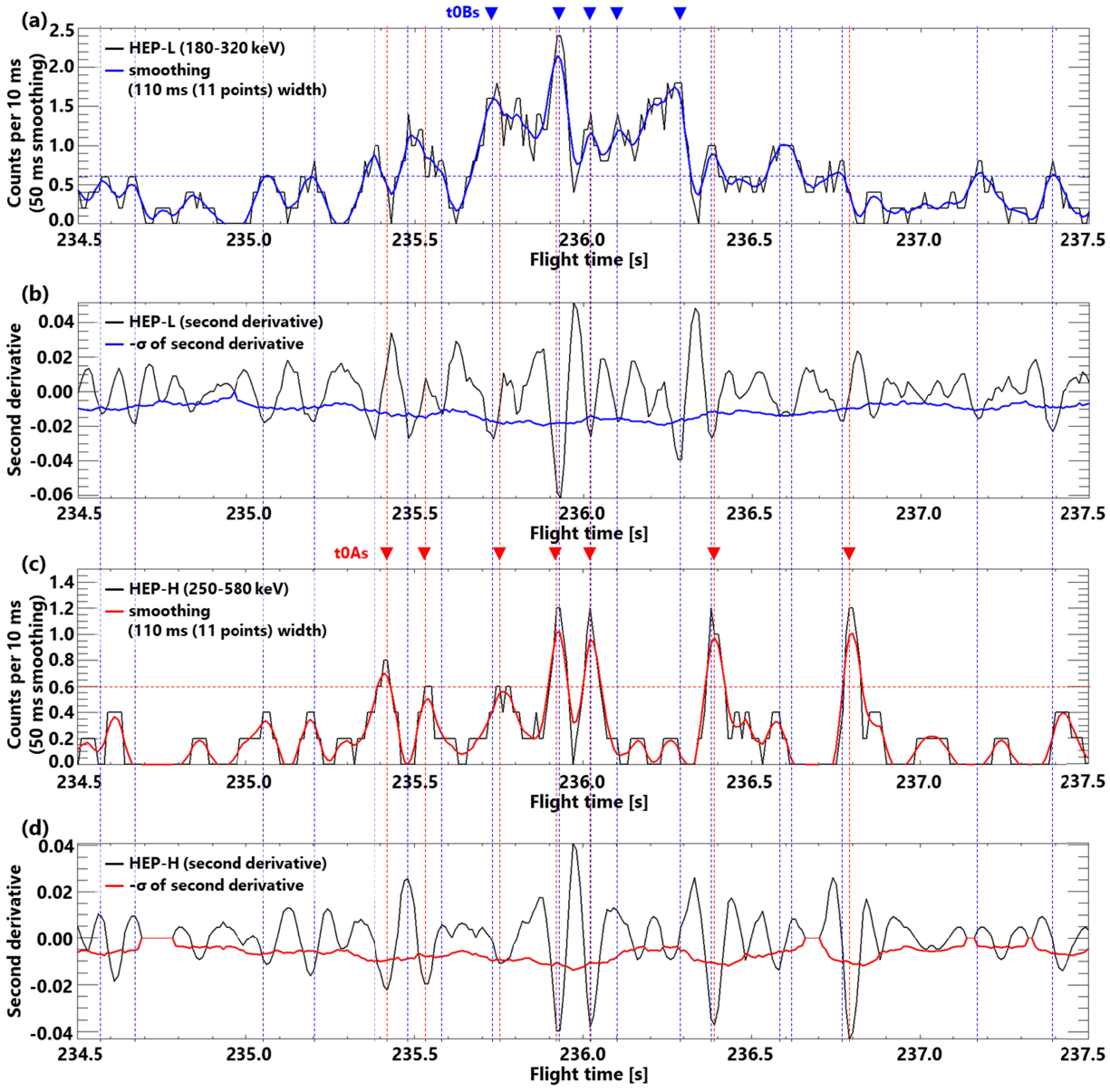

Figure 2. (a) and (c): The electron count rates (HEP-L and HEP-H) together with the smoothed values with time windows of 110 ms. The electron count rates plotted in Figures 2a and 2c are the same as those in Figures 1e and 1f. (b) and (d): The second time derivatives of the smoothed count rate and their standard deviations assuming randomness and independence of each count rate data. The blue and red dotted lines show the appearance timings of identified bursts. The red and blue triangles (called t0As and t0Bs) indicate reference timings of the superpositions shown in Figures 3b and 3c.

Correlation coefficients on time profiles of microbursts between HEP-H and HEP-L were calculated to demonstrate the relevance of each burst. The correlation coefficients were calculated with a sliding window 600 ms wide, successively moved by 10 ms during the period from 235 to 237 s after the launch of LAMP. The HEP-H data were shifted with respect to the HEP-L electron data within ±100 ms to examine changes in the correlation coefficients. Figure 3a shows the calculated correlation coefficients. The vertical axis shows the shifted time of the HEP-H electron data, and the horizontal axis is the start time of each correlation coefficient calculation window. A positive time shift of the HEP-H data indicates that HEP-L precedes HEP-H. Figure 3a demonstrates that the significant correlation coefficients appear when the HEP-H data are positively shifted in time, indicating that HEP-L tends to precede HEP-H at 235.0–237.0 s after the launch of LAMP. Particularly large correlation coefficients (>0.5) are obtained when the HEP-L data precedes by 30 ms at 235.0 to 235.3 s and by 0–10 ms at 235.3 to 235.7 s. This characteristic is consistent with that of the analysis by simple identification of the appearance timings of the HEP-H and HEP-L microbursts described in Figure 2. Note that the result of correlation coefficient calculation is more susceptible to bursts with higher count rates in the calculation window.

A superposed epoch analysis was applied to bursts detected by both HEP-H and HEP-L to accurately estimate the appearance time lag between them. In this analysis, the reference time (t=0) is set as the timing when peaks of microbursts are identified in the HEP-H data, which is indicated by the red triangles (t0As) in Figure 2c. The result of the superposed epoch analysis is shown in Figure 3b. The time range of superposition is ±70 ms from the reference timing. A significant enhancement of HEP-L precedes that of HEP-H, with a time lag of 10 ms between peak appearances. Red and black dotted lines in Figure 3b indicate when the enhancements of counts of HEP-H and HEP-L reach 50% of their peaks, respectively. These values for HEP-L appear at 18.3 ms and 25.4 ms before those of HEP-H, respectively. This result also suggests that most of the microbursts at the HEP-L appear before the microbursts at the HEP-H, indicating the inverse energy dispersion feature of the observed microburst. Then, a similar superposed epoch analysis was performed on the EPLAS-H/M/L data to investigate the precipitation timing of lower-energy electrons relative to those of microbursts at the HEP-L and HEP-H. The reference time is set as the timing when peaks of microbursts at the HEP-L are identified (blue triangles (t0Bs) in Figure 2a). The microbursts at the HEP-L selected as t0Bs are obtained in the core of the microburst train and are most suitable for comparison with the low-energy electron precipitation train. Figure 3c shows the results of the analysis. An increase in count rates appears in the order of EPLAS-H, EPLAS-M, and EPLAS-L. The time lags from t0Bs are 546, 672, and 840 ms for the peaks of EPLAS-H, EPLAS-M, and EPLAS-L, respectively.

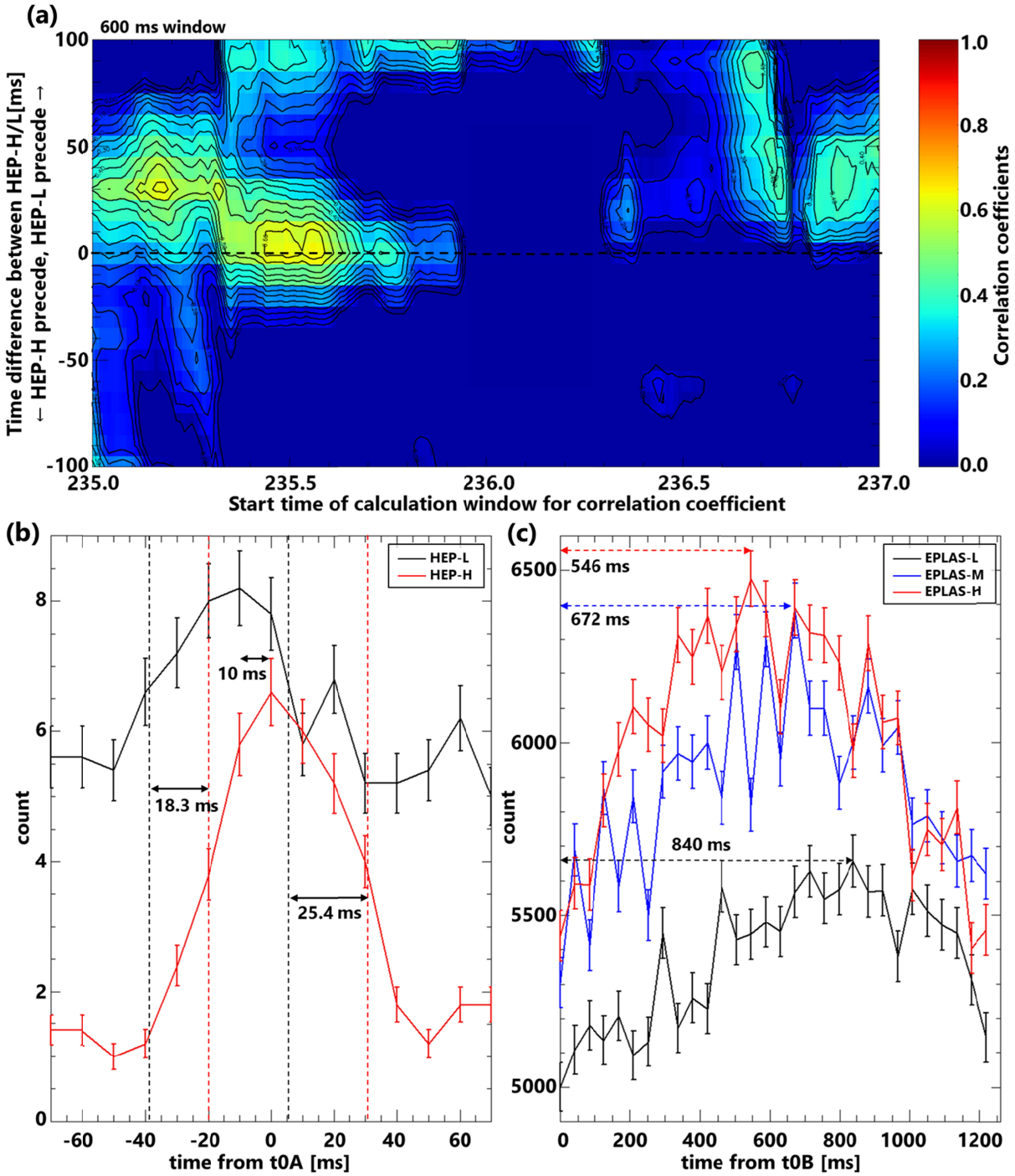

Figure 3. (a) Correlation coefficients between HEP-H and HEP-L calculated every 10 ms with a time window of 600 ms. The contours are also plotted every 0.05. (b) Calculated HEP-H (red) and HEP-L (black) by the superposed epoch analysis. The reference time (t=0) is set as the timing when peaks of HEP-H microbursts are identified (t0As in Figure 2). Red and black dotted lines indicate when the enhancements of HEP-H and HEP-L reach halves of their peaks, respectively. (c) Calculated EPLAS-H (red line), EPLAS-M (black line), and EPLAS-L (blue

line) by the superposed epoch analysis. The reference time (t=0) is set as the timing when peaks of HEP-L bursts are identified (t0Bs in Figure 2).

4 Discussion

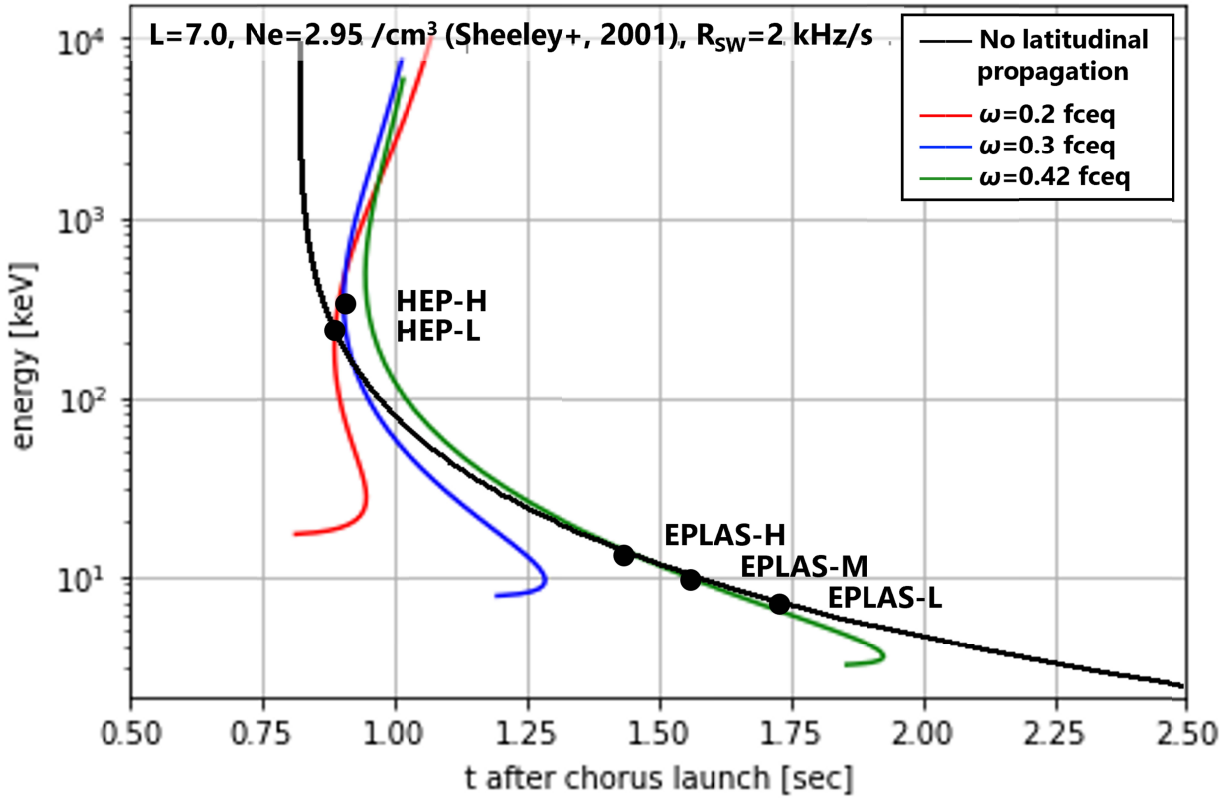

Figure 4. Arrival timings of precipitating electrons at the ionospheric altitude as a function of electron energies. Black dots show the timings obtained by the LAMP observations. Red, blue, and green lines show timings based on the theory of Miyoshi et al. (2010) and Saito et al. (2012), where the frequency of waves at wave launch (ω) is 0.2, 0.3, and 0.42 $f_{c,eq}$, respectively. A black line shows calculated timings assuming electrons of all energies with a pitch angle of 0 degrees depart from the magnetic equator at the same time. Note that the timings obtained by the observation are plotted so that the peak timing of HEP-L microbursts matches the calculated timing of the electron precipitation with energies of 240 keV based on the simulation for ω = 0.2 $f_{c,eq}$.

Here, we compare the energy-time dispersion of the precipitating electron fluxes observed by LAMP with those deduced from numerical simulations. Based on the theory about pitch angle scattering of pulsating aurora and microbursts [Miyoshi et al., 2015, 2020; Saito et al., 2012], we calculated the elapsed time from the generation of chorus waves at the equatorial magnetosphere to the arrival of precipitating electrons at the ionospheric altitude. For the generation of chorus waves, we launched a single rising tone element of chorus waves at the equator with a frequency sweep rate of 2 kHz/s. In the simulation, the background electron

density in the magnetosphere is assumed as 2.95 cm^{-3}, which is uniformly distributed along the magnetic field line using the model of Sheeley et al. (2001).

Figure 4 shows the arrival timings of precipitating electrons at the ionospheric altitude as a function of electron energies. Red, blue, and green lines show calculated timings by the test particle simulation, where the frequency of waves at the wave launch (ω) is 0.2, 0.3, and 0.42 $f_{c,eq}$ ($f_{c,eq}$ is electron cyclotron angular frequency at the equator where the waves are launched), respectively. On the other hand, black dots indicate the observed timings which are plotted so that the peak timing of microbursts at the HEP-L matches the calculated timing of the electron precipitation with energies of 240 keV based on the simulation for $\omega = 0.2\, f_{c,eq}$. Note that dots for the microbursts at the HEP-L and HEP-H are plotted at energies 380 and 240 keV, respectively. In the plot, we take 20 ms for the time lag between the appearance of the microbursts at the HEP-L and HEP-H. The inverse energy-time dispersion observed by HEP is in good agreement with the numerical simulation for $\omega=0.2\, f_{c,eq}$, and the observed peak timings of electron flux enhancement around 10 keV are consistent with the simulation for $\omega=0.42\, f_{c,eq}$. This mixture of multiple results is caused by the rising tone element of chorus waves which has certain frequency bandwidth at the same time [e.g., Santolík et al., 2003]. Note that the results may have been some ambiguities by the non-uniformity of the frequency chirping rate of the rising tones, as well as amplitude fluctuations during chirping and phase discontinuities. Also, the differences in arrival timings of observed electrons with energies around 10 keV are longer than those with energies 380 and 240 keV. This feature suggests that a flux enhancement of electrons with energies around 10 keV has a longer time scale than that of electrons with energies of a few hundred keV. These are consistent with the simulation results of Miyoshi et al. (2020).

The black line shows the timings assuming electrons of all energies with a pitch angle of 0 degrees depart from the magnetic equator at the same time. This assumption corresponds to the case that the pitch angle scatterings of all energy electrons take place at the magnetic equator. In this case, the 380 keV electrons are shown to arrive before the 240 keV electrons, which is not consistent with the observed energy-time dispersion.

5 Conclusions

The energy-time dispersion of precipitating electrons in the pulsating auroral patch was identified by in-situ observations with the energy range from 6.7 keV to 580 keV range for the first time. At energies above 180 keV, the observed microbursts show the inverse energy-time dispersion. The observed energy-time dispersion is consistent with the theoretical model. This observation is consistent with the model that relativistic electron microbursts are a high-energy tail of pulsating aurora; the pitch angle scattering of electrons by chorus waves generates the microburst precipitation of relativistic/sub-relativistic electrons as well as the precipitation of lower-energy electrons which is responsible for the photon emission of pulsating auroras.

Acknowledgments

We are grateful for the support of NASA Wallops Flight Facility (WFF) and Poker Flat Research Range (PFRR). This work was supported by the Japan Society for the Promotion of Science

(JSPS), KAKENHI (15H05747, 18KK0100, 20H01959, 21H04526, 22H00173, and 22KK0046). This work was carried out by the joint research program of the Institute for Space−Earth Environmental Research (ISEE), Nagoya University. We thank Kolya Tsyganenko for his Geopack and external magnetic field model routines.

Data Availability Statement

The data from the rocket and instruments (HEP, EPLAS, and AIC) used in this study are available at the UTokyo Repository (https://repository.dl.itc.u-tokyo.ac.jp/records/2007295). The data from the ground-based all-sky cameras are available at https://ergsc.isee.nagoya-u.ac.jp/psa-pwing/pub/raw/lamp/sav_img/. Note that all of the data publication links related with the LAMP sounding rocket experiment are temporary for the reviewers and will be changed to official data publication sites with DOIs by the publishment of this paper. Detectable energy range of HEP for electrons was estimated based on the ESTAR web database of electron stopping powers and ranges provided by the National Institutes of Standards and Technology (NIST) [Berger et al., 2017]. The incident energies of the electrons detected by HEP were calculated with the Geant4 toolkit [Agostinelli et al., 2003; Allison et al., 2006: Allison et al., 2016]. The magnetic coordinate system is calculated by the IGRF-13 model (https://www.ngdc.noaa.gov/IAGA/vmod/igrf.html). The present study used SPEDAS for data analysis [Angelopoulos et al., 2019].

References

Agostinelli, S., Allison, J., Amako, K., Apostolakis, J., Araujo, H., Arce, P., et al. (2003). Geant4—a simulation toolkit. *Nuclear Instruments and Methods in Physics Research Section A: Accelerators, Spectrometers, Detectors and Associated Equipment*, *506*(3), 250–303. https://doi.org/10.1016/S0168-9002(03)01368-8

Allison, J., Amako, K., Apostolakis, J., Araujo, H., Arce Dubois, P., Asai, M., et al. (2006). Geant4 developments and applications. *IEEE Transactions on Nuclear Science*, *53*(1), 270–278. https://doi.org/10.1109/TNS.2006.869826

Allison, J., Amako, K., Apostolakis, J., Arce, P., Asai, M., Aso, T., et al. (2016). Recent developments in Geant4. *Nuclear Instruments and Methods in Physics Research Section A: Accelerators, Spectrometers, Detectors and Associated Equipment*, *835*, 186–225. https://doi.org/10.1016/j.nima.2016.06.125

Angelopoulos, V., Cruce, P., Drozdov, A., Grimes, E. W., Hatzigeorgiu, N., King, D. A., et al. (2019). The Space Physics Environment Data Analysis System (SPEDAS). *Space Science Reviews*, *215*(1), 9. https://doi.org/10.1007/s11214-018-0576-4

Berger, M. J., Coursey, J. S, Zucker, M. A., and Chang, J. (2017). NIST Standard Reference Database 124. https://dx.doi.org/10.18434/T4NC7P

Blake, J. B., Looper, M. D., Baker, D. N., Nakamura, R., Klecker, B., & Hovestadt, D. (1996). New high temporal and spatial resolution measurements by SAMPEX of the precipitation of relativistic electrons. *Advances in Space Research*, *18*(8), 171–186. https://doi.org/10.1016/0273-1177(95)00969-8

Blum, L., Li, X., & Denton, M. (2015). Rapid MeV electron precipitation as observed by SAMPEX/HILT during high-speed stream-driven storms. *Journal of Geophysical Research: Space Physics*, *120*(5), 3783–3794. https://doi.org/10.1002/2014JA020633

Breneman, A. W., Crew, A., Sample, J., Klumpar, D., Johnson, A., Agapitov, O., et al. (2017). Observations Directly Linking Relativistic Electron Microbursts to Whistler Mode Chorus: Van Allen Probes and FIREBIRD II. *Geophysical Research Letters*, *44*(22), 11,265-11,272. https://doi.org/10.1002/2017GL075001

Clilverd, M. A., Rodger, C. J., & Ulich, T. (2006). The importance of atmospheric precipitation in storm-time relativistic electron flux drop outs. *Geophysical Research Letters*, *33*(1), n/a-n/a. https://doi.org/10.1029/2005GL024661

Datta, S., Skoug, R. M., McCarthy, M. P., & Parks, G. K. (1997). Modeling of microburst electron precipitation using pitch angle diffusion theory. *Journal of Geophysical Research: Space Physics*, *102*(A8), 17325–17333. https://doi.org/10.1029/97JA00942

Dietrich, S., Rodger, C. J., Clilverd, M. A., Bortnik, J., & Raita, T. (2010). Relativistic microburst storm characteristics: Combined satellite and ground-based observations. *Journal of Geophysical Research: Space Physics*, *115*(A12), n/a-n/a. https://doi.org/10.1029/2010JA015777

Douma, E., Rodger, C. J., Blum, L. W., O'Brien, T. P., Clilverd, M. A., & Blake, J. B. (2019). Characteristics of Relativistic Microburst Intensity From SAMPEX Observations. *Journal of Geophysical Research: Space Physics*, *124*(7), 5627–5640. https://doi.org/10.1029/2019JA026757

Douma, Emma, Rodger, C. J., Blum, L. W., & Clilverd, M. A. (2017). Occurrence characteristics of relativistic electron microbursts from SAMPEX observations. *Journal of Geophysical Research: Space Physics*, *122*(8), 8096–8107. https://doi.org/10.1002/2017JA024067

Duderstadt, K. A., Huang, C. -L., Spence, H. E., Smith, S., Blake, J. B., Crew, A. B., et al. (2021). Estimating the Impacts of Radiation Belt Electrons on Atmospheric Chemistry Using FIREBIRD II and Van Allen Probes Observations. *Journal of Geophysical Research: Atmospheres*, *126*(7). https://doi.org/10.1029/2020JD033098

Horne, R. B., & Thorne, R. M. (2003). Relativistic electron acceleration and precipitation during resonant interactions with whistler-mode chorus. *Geophysical Research Letters*, *30*(10), n/a-n/a. https://doi.org/10.1029/2003GL016973

Hosokawa, K., Miyoshi, Y., Ozaki, M., Oyama, S.-I., Ogawa, Y., Kurita, S., et al. (2020). Multiple time-scale beats in aurora: precise orchestration via magnetospheric chorus waves. *Scientific Reports*, *10*(1), 3380. https://doi.org/10.1038/s41598-020-59642-8

Kasahara, S., Miyoshi, Y., Yokota, S., Mitani, T., Kasahara, Y., Matsuda, S., et al. (2018). Pulsating aurora from electron scattering by chorus waves. *Nature*, *554*(7692), 337–340. https://doi.org/10.1038/nature25505

Kawamura, M., Sakanoi, T., Fukizawa, M., Miyoshi, Y., Hosokawa, K., Tsuchiya, F., et al. (2021). Simultaneous Pulsating Aurora and Microburst Observations With Ground-Based Fast Auroral Imagers and CubeSat FIREBIRD-II. *Geophysical Research Letters*, *48*(18). https://doi.org/10.1029/2021GL094494

Kurita, S., Miyoshi, Y., Blake, J. B., Reeves, G. D., & Kletzing, C. A. (2016). Relativistic electron microbursts and variations in trapped MeV electron fluxes during the 8–9 October 2012 storm: SAMPEX and Van Allen Probes observations. *Geophysical Research Letters*, *43*(7), 3017–3025. https://doi.org/10.1002/2016GL068260

Lorentzen, K. R., Looper, M. D., & Blake, J. B. (2001). Relativistic electron microbursts during the GEM storms. *Geophysical Research Letters*, *28*(13), 2573–2576. https://doi.org/10.1029/2001GL012926

Miyoshi, Y, Katoh, Y., Nishiyama, T., Sakanoi, T., Asamura, K., & Hirahara, M. (2010). Time of flight analysis of pulsating aurora electrons, considering wave-particle interactions with propagating whistler mode waves. *Journal of Geophysical Research: Space Physics*, *115*(A10), n/a-n/a. https://doi.org/10.1029/2009JA015127

Miyoshi, Y., Oyama, S., Saito, S., Fujiwara, H., Kataoka, R., Ebihara, Y., Kletzing, C., Reeves, G., Santolik, O., Cliverd, M., Rodger, C., Turunen, E., Tsuchiya, F. (2015a). Energetic electron precipitation associated with pulsating aurora: EISCAT and Van Allen Probes observations, *Journal of Geophysical Research*, 120, doi:10.1002/2014JA020690

Miyoshi, Y., S. Saito, K.Seki, T. Nishiyama, R. Kataoka, K. Asamura, Y. Katoh, Y. Ebihara, T. Sakanoi, M. Hirahara, S. Oyama, S. Kurita, and O. Santolik, (2015b). Relation between energy spectra of pulsating aurora electrons and frequency spectra of whistler-mode chorus waves, *Journal of Geophysical Research*, 120, 7728-7736, doi:10.1002/2015JA021562, 2015.

Miyoshi, Y., Saito, S., Kurita, S., Asamura, K., Hosokawa, K., Sakanoi, T., et al. (2020). Relativistic Electron Microbursts as High-Energy Tail of Pulsating Aurora Electrons. *Geophysical Research Letters*, *47*(21). https://doi.org/10.1029/2020GL090360

Miyoshi, Y., K. Hosokawa, S. Kurita, S.-I. Oyama, Y. Ogawa, S. Saito, I. Shinohara, A. Kero, E. Turunen, P. T. Verronen, S. Kasahara, S. Yokota, T. Mitani, T. Takashima, N. Higashio, Y. Kasahara, S. Masuda, F. Tsuchiya, A. Kumamoto, A. Matsuoka, T. Hori, K. Keika, M. Shoji, M. Teramoto, S. Imajo, C. Jun, and S. Nakamura, (2021). Penetration of MeV electrons into the mesosphere accompanying pulsating aurorae, *Scientific Reports*, 11, 13724, doi:10.1038/s41598-021-92611-3

Nakamura, R., Baker, D. N., Blake, J. B., Kanekal, S., Klecker, B., & Hovestadt, D. (1995). Relativistic electron precipitation enhancements near the outer edge of the radiation belt. *Geophysical Research Letters*, *22*(9), 1129–1132. https://doi.org/10.1029/95GL00378

Nakamura, R., Isowa, M., Kamide, Y., Baker, D. N., Blake, J. B., & Looper, M. (2000). SAMPEX observations of precipitation bursts in the outer radiation belt. *Journal of Geophysical Research: Space Physics*, *105*(A7), 15875–15885. https://doi.org/10.1029/2000JA900018

Namekawa, T., Mitani, T., Asamura, K., Miyoshi, Y., Hosokawa, K., Ogawa, Y., et al. (2021). Rocket Observation of Sub-Relativistic Electrons in the Quiet Dayside Auroral Ionosphere. *Journal of Geophysical Research: Space Physics*, *126*(7), 1–13. https://doi.org/10.1029/2020JA028633

Nishimura, Y., Bortnik, J., Li, W., Thorne, R. M., Chen, L., Lyons, L. R., et al. (2011), Multievent study of the correlation between pulsating aurora and whistler mode chorusemissions, *Journal of Geophysical Research*,116, A11221, doi:10.1029/2011JA016876

O'Brien, T. P. (2003). Energization of relativistic electrons in the presence of ULF power and MeV microbursts: Evidence for dual ULF and VLF acceleration. *Journal of Geophysical Research*, *108*(A8), 1329. https://doi.org/10.1029/2002JA009784

O'Brien, T. P. (2004). Quantification of relativistic electron microburst losses during the GEM storms. *Geophysical Research Letters*, *31*(4), L04802. https://doi.org/10.1029/2003GL018621

Oliven, M. N., & Gurnett, D. A., (1968). Microburst phenomena: 3. An association between microbursts and VLF chorus. *Journal of Geophysical Research*,*73*(7), 2355-2362. https://doi.org/10.1029/JA073i007p02355

Oyama, S., Kero, A., Rodger, C. J., Clilverd, M. A., Miyoshi, Y., Partamies, N., et al. (2017). Energetic electron precipitation and auroral morphology at the substorm recovery phase. *Journal of Geophysical Research: Space Physics*, *122*(6), 6508–6527. https://doi.org/10.1002/2016JA023484

Ozaki, M., Miyoshi, Y., Shiokawa, K., Hosokawa, K., Oyama, S., Kataoka, R., et al. (2019). Visualization of rapid electron precipitation via chorus element wave–particle interactions. *Nature Communications*, *10*(1), 257. https://doi.org/10.1038/s41467-018-07996-z

Saito, S., Miyoshi, Y., & Seki, K. (2012). Relativistic electron microbursts associated with whistler chorus rising tone elements: GEMSIS-RBW simulations. *Journal of Geophysical Research: Space Physics*, *117*(A10), n/a-n/a. https://doi.org/10.1029/2012JA018020

Sandahl, I., Eliasson, L., & Lundin, R. (1980). Rocket observations of precipitating electrons over a pulsating aurora. *Geophysical Research Letters*, *7*(5), 309–312. https://doi.org/10.1029/GL007i005p00309

Santolík, O., Gurnett, D. A., Pickett, J. S., Parrot, M., & Cornilleau-Wehrlin, N., (2003). Spatio-temporal structure of storm-time chorus, *Journal of Geophysical Research*, 108(A7), 1278, https://doi.org/10.1029/2002JA009791

Savitzky, A., & Golay, M. J. E., (1964). Smoothing and Differentiation of Data by Simplified Least Squares Procedures. *Anal. Chem.,* 1964, 36, 8, 1627–1639. https://doi.org/10.1021/ac60214a047

Seppälä, A., Douma, E., Rodger, C. J., Verronen, P. T., Clilverd, M. A., & Bortnik, J. (2018). Relativistic Electron Microburst Events: Modeling the Atmospheric Impact. *Geophysical Research Letters*, *45*(2), 1141–1147. https://doi.org/10.1002/2017GL075949

Sheeley, B. W., Moldwin, M. B., Rassoul, H. K., & Anderson, R. R. (2001). An empirical plasmasphere and trough density model: CRRES observations. *Journal of Geophysical Research: Space Physics*, *106*(A11), 25631–25641. https://doi.org/10.1029/2000JA000286

Shumko, M., Gallardo-Lacourt, B., Halford, A. J., Liang, J., Blum, L. W., Donovan, E., et al. (2021a). A Strong Correlation Between Relativistic Electron Microbursts and Patchy Aurora. *Geophysical Research Letters*, *48*(18). https://doi.org/10.1029/2021GL094696

Shumko, M., Blum, L. W., & Crew, A. B. (2021b). Duration of Individual Relativistic Electron Microbursts: A Probe Into Their Scattering Mechanism. *Geophysical Research Letters*, *48*(17). https://doi.org/10.1029/2021GL093879

Shumko, Mykhaylo, Sample, J., Johnson, A., Blake, B., Crew, A., Spence, H., et al. (2018). Microburst Scale Size Derived From Multiple Bounces of a Microburst Simultaneously Observed With the FIREBIRD-II CubeSats. *Geophysical Research Letters*, *45*(17), 8811–8818. https://doi.org/10.1029/2018GL078925

Thébault, E., Finlay, C. C., Beggan, C. D., Alken, P., Aubert, J., Barrois, O., et al. (2015). International Geomagnetic Reference Field: the 12th generation. *Earth, Planets and Space*, *67*(1), 79. https://doi.org/10.1186/s40623-015-0228-9

Thorne, R. M., O'Brien, T. P., Shprits, Y. Y., Summers, D., & Horne, R. B. (2005). Time-scale for MeV electron microburst loss during geomagnetic storms. *Journal of Geophysical Research: Space Physics*, *110*(A9), 1–7. https://doi.org/10.1029/2004JA010882

Verronen, P. T., Kero, A., Partamies, N., Szeląg, M. E., Oyama, S.-I., Miyoshi, Y., & Turunen, E. (2021). Simulated seasonal impact on middle atmospheric ozone from high-energy

electron precipitation related to pulsating aurorae. *Annales Geophysicae*, *39*(5), 883–897. https://doi.org/10.5194/angeo-39-883-2021